Journal of Zhejiang University-SCIENCE A (Applied Physics & Engineering)
ISSN 1673-565X (Print); ISSN 1862-1775 (Online)
www.zju.edu.cn/jzus; www.springerlink.com
E-mail: jzus@zju.edu.cn

Analysis of the penalty version of the Arlequin framework for the prediction of structural responses with large deformations*

Hua QIAO, Wei-qiu CHEN†‡

(*Department of Engineering Mechanics, Zhejiang University, Hangzhou 310027, China*)

†E-mail: chenwq@zju.edu.cn

Received Dec. 25, 2010; Revision accepted May 14, 2011; Crosschecked June 21, 2011

Abstract: The Arlequin framework proposed by Ben Dhia in 1998 is a flexible and robust method for conducting global/local analysis of structures and materials. A penalty version of the Arlequin framework for the study of structural problems involving large deformation is considered here. The implementation of the penalty-based Arlequin framework into ABAQUS is then explored and the corresponding Arlequin user element subroutine is developed. Geometric nonlinear simulations of a cantilever beam and a shallow arch are conducted and the choice of the coupling operator with an appropriate penalty parameter is studied. The numerical results justify the feasibility of the proposed method, ensuring its further application to more complicated problems involving geometric or material nonlinearities.

Key words: Global/Local analysis, Geometric nonlinear analysis, Penalty-based Arlequin method, User defined element
doi:10.1631/jzus.A1000519 **Document code:** A **CLC number:** O342

1 Introduction

Multi-scale simulation of materials and structures is one of the most active research areas in the 21st century in the fields of material sciences, aeronautical and astronautical engineering, mechanical manufacturing industry, and civil engineering, etc. A large amount of studies have been carried out on multi-scale simulation of materials, but much less research has been done on the simulation of structures. The global/local analysis of structures is considered to be, in a general sense, a particular multi-scale method, and is necessary for efficient and accurate analysis of complicated problems especially in recognizing the evolution process of the failure of structures. In those cases, the conventional mono-model simulation is not suitable due to the fact that the final failure of structures is related to the global response under external forces as well as to the local damage accumulation. Some approaches for global/local analysis of structures have been developed, including the variational multi-scale (VMS) method (Hughes, 1995), the mesh superposition (MS) method (Fish, 1992), the multi-grid (MG) technique (Rannou *et al*., 2009), the iterative global/local (IGL) technique (Whitcomb and Woo, 1993), the multi-point constraint method (Voleti *et al*., 1996), and the Arlequin method (Ben Dhia, 1998). Among all the methods mentioned above, the Arlequin method is perhaps the most flexible and promising one. It can be used to couple two different mechanical states to conduct global/local analyses, using reliable energy partition function and coupling operators.

The mathematical aspects of the Arlequin method were presented within the framework of linear elasticity (Ben Dhia and Rateau, 2001; Ben Dhia, 2008). The application of the method to various linear elastic problems was also discussed in Ben Dhia and

‡ Corresponding author

* Project supported by the National Natural Science Foundation of China (No. 10725210) and the National Basic Research Program (973) of China (No. 2009CB623200)

Rateau (2005), Guidault and Belytschko (2007), and Hu *et al*. (2008). Ben Dhia and Zammali (2004) considered dynamic contact problems using the Arlequin framework. Hu *et al*. (2010) proposed a global/local geometric nonlinear analysis of sandwich structures by combining the nonlinear Arlequin framework with the asymptotic numerical method and the nonlinear analysis scheme was derived using the total Lagrangian formulation. In order to have great flexibility, high reliability, and efficiency when conducting global/local analyses of large or complex structures of interest in civil engineering, implementation of the Arlequin method into the commercial finite element software ABAQUS has been attempted in Qiao *et al*. (2010; 2011).

The existence and uniqueness of solutions to continuous penalty-based Arlequin problems were proved by Ben Dhia (2008). However, the applications of the Arlequin method mentioned above all adopt the Lagrange multiplier to couple two mechanical states. In the present study, we focus on the implementation of the penalty-based Arlequin method into ABAQUS for geometric nonlinear analyses of structures and study how to select suitable coupling operators. We also investigate the effects that the selection of penalty parameters may have on numerical results.

2 Penalty-based Arlequin method

We consider a body occupying a domain $\Omega \subset \mathbb{R}^d$, d=2 or 3, subjected to body forces $\boldsymbol{f}$ and kinematic boundary conditions on the portion Γ_u of the boundary $\partial\Omega$. In order to apply the Arlequin method, we divide the domain Ω into subdomains $\Omega_1\backslash\Omega_0$, $\Omega_2\backslash\Omega_0$, and Ω_0 with $\Omega_0=\Omega_1\cap\Omega_2\neq\varnothing$ and $\Omega=\Omega_1\cup\Omega_2$. We denote the configurations of the subdomains at time t as ${}^t\Omega_1\backslash{}^t\Omega_0$, ${}^t\Omega_2\backslash{}^t\Omega_0$, and ${}^t\Omega_0$, as shown in Fig. 1.

Suppose that the subdomain ${}^t\Omega_1$ is discretized with coarse meshes and ${}^t\Omega_2$ is discretized with fine meshes. The penalty method will be adopted to couple the coarse and fine meshes in the coupling zone ${}^t\Omega_0$. For simplicity, we assume that no surface tractions are applied on the boundary $\partial\Omega$.

The total energy ${}^{t+\Delta t}_{t}E_{\mathrm{tol}}$ of the coupled model at time t+Δt with respect to the configuration at time t is given by

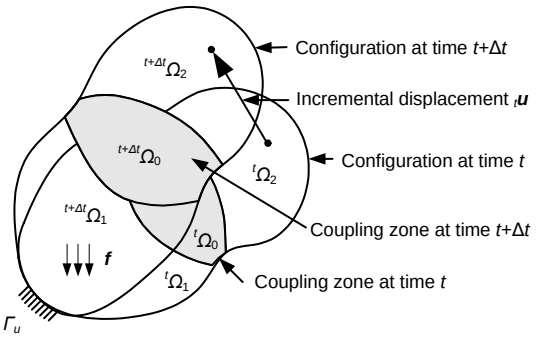

Fig. 1 Subdomain configurations with an overlapping zone at times t and t+Δt

$$
\begin{aligned}
{}^{t+\Delta t}_{t}E_{\mathrm{tol}} = {}&{}^{t+\Delta t}_{t}E_1({}_t\boldsymbol{u}_1)+{}^{t+\Delta t}_{t}E_2({}_t\boldsymbol{u}_2)\\
&+C({}_t\boldsymbol{u}_1-{}_t\boldsymbol{u}_2,{}_t\boldsymbol{u}_1-{}_t\boldsymbol{u}_2),
\end{aligned}
\tag{1}
$$

where ${}_t\boldsymbol{u}_i$ denotes the incremental displacement from time t to t+Δt in the domain Ω_i, C is a linear coupling operator, ${}^{t+\Delta t}_{t}E_i$ is the weighted potential energy in the domain Ω_i at time t+Δt with respect to the configuration at time t, and we have

$$
\begin{aligned}
{}^{t+\Delta t}_{t}E_1 = {}&\alpha_1\int_{{}^t\Omega_1}\frac{1}{2}{}^{t+\Delta t}_{t}\boldsymbol{S}({}_t\boldsymbol{u}_1):{}^{t+\Delta t}_{t}\boldsymbol{\varepsilon}({}_t\boldsymbol{u}_1)\mathrm{d}\,{}^t\Omega\\
&-\int_{{}^t\Omega_1}\beta_1{}^{t+\Delta t}_{t}\boldsymbol{f}\cdot{}_t\boldsymbol{u}_1\mathrm{d}\,{}^t\Omega,
\end{aligned}
\tag{2}
$$

$$
\begin{aligned}
{}^{t+\Delta t}_{t}E_2 = {}&\alpha_2\int_{{}^t\Omega_2}\frac{1}{2}{}^{t+\Delta t}_{t}\boldsymbol{S}({}_t\boldsymbol{u}_2):{}^{t+\Delta t}_{t}\boldsymbol{\varepsilon}({}_t\boldsymbol{u}_2)\mathrm{d}\,{}^t\Omega\\
&-\int_{{}^t\Omega_2}\beta_2{}^{t+\Delta t}_{t}\boldsymbol{f}\cdot{}_t\boldsymbol{u}_2\mathrm{d}\,{}^t\Omega,
\end{aligned}
\tag{3}
$$

where ${}^{t+\Delta t}_{t}\boldsymbol{S}$ and ${}^{t+\Delta t}_{t}\boldsymbol{\varepsilon}$ are, respectively, the Kirchhoff stress and Green strain tensors at time t+Δt corresponding to the configuration at time t; α_i and β_i are, respectively, weight functions for strain energy and work due to external force in domain Ω_i and satisfy the following relations:

$$\alpha_1+\alpha_2=\beta_1+\beta_2=1. \tag{4}$$

Eq. (4) allows a relatively flexible scheme for energy partition between the two models. In this study, we propose to use the penalty method and the coupling operator in Eq. (1) may be expressed as

$$C({}_t\boldsymbol{u}_1-{}_t\boldsymbol{u}_2,{}_t\boldsymbol{u}_1-{}_t\boldsymbol{u}_2)=\frac{1}{2}k\int_{{}^0\Omega_0}({}_t\boldsymbol{u}_1-{}_t\boldsymbol{u}_2)\cdot({}_t\boldsymbol{u}_1-{}_t\boldsymbol{u}_2)\mathrm{d}^0\Omega_0, \tag{5}$$

where k is the penalty parameter corresponding to the incremental displacement. Here, the configuration at time 0, ${}^0\Omega_0$, rather than those at time t, ${}^t\Omega_0$, should be used since the domains Ω_1 and Ω_2, which overlap in the coupling zone at time 0, may slightly drift apart from each other in the coupling zone at time t due to the weak and flexible coupling required in the Arlequin framework, as shown in Fig. 2. Thus, in order to avoid the error accumulation during the nonlinear solving procedure, one calculates the coupling matrices according to the configuration at time 0 to assure the reliable coupling at each time step.

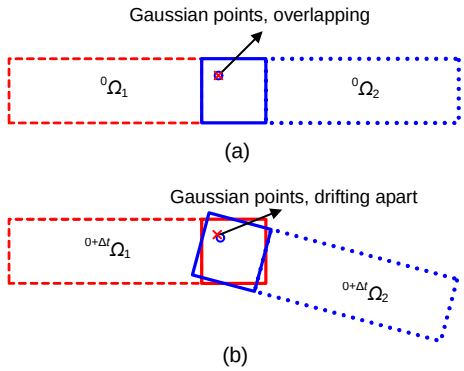

Fig. 2 Sketch for the drifting apart phenomenon
(a) Configuration at time 0; (b) Configuration at time $0+\Delta t$

Applying the principle of virtual work for a deformable body, we can obtain

$$\alpha_1\int_{{}_t\Omega_1}{}_t^{t+\Delta t}\boldsymbol{S}({}_t\boldsymbol{u}_1):{}_t^{t+\Delta t}\boldsymbol{\varepsilon}(\delta{}_t\boldsymbol{u}_1)\mathrm{d}^t\Omega+C({}_t\boldsymbol{u}_1-{}_t\boldsymbol{u}_2,\delta{}_t\boldsymbol{u}_1)=\int_{\Omega_1}\beta_1{}_t^{t+\Delta t}\boldsymbol{f}\cdot\delta{}_t\boldsymbol{u}_1\mathrm{d}^t\Omega,\quad\forall\delta{}_t\boldsymbol{u}_1\in W_1, \tag{6}$$

$$\alpha_2\int_{\Omega_2}{}_t^{t+\Delta t}\boldsymbol{S}({}_t\boldsymbol{u}_2):{}_t^{t+\Delta t}\boldsymbol{\varepsilon}(\delta{}_t\boldsymbol{u}_2)\mathrm{d}^t\Omega-C({}_t\boldsymbol{u}_1-{}_t\boldsymbol{u}_2,\delta{}_t\boldsymbol{u}_2)=\int_{\Omega_2}\beta_2{}_t^{t+\Delta t}\boldsymbol{f}\cdot\delta{}_t\boldsymbol{u}_2\mathrm{d}^t\Omega,\quad\forall\delta{}_t\boldsymbol{u}_2\in W_2, \tag{7}$$

where δ denotes a virtual variation, and W_1 and W_2 denote the respective kinematically admissible spaces.

Using the incremental decompositions (Bathe, 1996), the Kirchhoff stress ${}_t^{t+\Delta t}\boldsymbol{S}$ and the Green strain ${}_t^{t+\Delta t}\boldsymbol{\varepsilon}$ can be written as

$${}_t^{t+\Delta t}\boldsymbol{S}={}^t\boldsymbol{\tau}+{}_t\boldsymbol{S}, \tag{8}$$

$${}_t^{t+\Delta t}\boldsymbol{\varepsilon}={}_t\boldsymbol{\varepsilon}={}_t\boldsymbol{e}+{}_t\boldsymbol{\eta}, \tag{9}$$

where ${}^t\boldsymbol{\tau}$ is the known Cauchy stress tensor at time t, ${}_t\boldsymbol{S}$ is the Kirchhoff incremental stress tensor, and ${}_t\boldsymbol{\varepsilon}$ is the incremental strain tensor corresponding to the configuration at time t, which can be written as the summation of the linear (${}_t\boldsymbol{e}$) and nonlinear (${}_t\boldsymbol{\eta}$) parts. For simplicity, the linearization assumption is employed:

$$\delta{}_t\boldsymbol{\varepsilon}=\delta{}_t\boldsymbol{e}. \tag{10}$$

Inserting Eqs. (8)–(10) into Eqs. (6) and (7), we have

$$\begin{aligned}&\alpha_1\int_{{}_t\Omega_1}{}_t\boldsymbol{S}({}_t\boldsymbol{u}_1):{}_t\boldsymbol{e}(\delta{}_t\boldsymbol{u}_1)\mathrm{d}^t\Omega+\alpha_1\int_{{}_t\Omega_1}{}^t\boldsymbol{\tau}({}_t\boldsymbol{u}_1):{}_t\boldsymbol{\eta}(\delta{}_t\boldsymbol{u}_1)\mathrm{d}^t\Omega\\&+\alpha_1\int_{{}_t\Omega_1}{}^t\boldsymbol{\tau}({}_t\boldsymbol{u}_1):{}_t\boldsymbol{e}(\delta{}_t\boldsymbol{u}_1)\mathrm{d}^t\Omega+k\int_{{}^0\Omega_0}({}_t\boldsymbol{u}_1-{}_t\boldsymbol{u}_2)\delta{}_t\boldsymbol{u}_1\mathrm{d}^0\Omega\\&=\int_{{}_t\Omega_1}\beta_1{}_t^{t+\Delta t}\boldsymbol{f}\cdot\delta{}_t\boldsymbol{u}_1\mathrm{d}^t\Omega,\quad\forall\delta{}_t\boldsymbol{u}_1\in W_1,\end{aligned} \tag{11}$$

$$\begin{aligned}&\alpha_2\int_{{}_t\Omega_2}{}_t\boldsymbol{S}({}_t\boldsymbol{u}_2):{}_t\boldsymbol{e}(\delta{}_t\boldsymbol{u}_2)\mathrm{d}^t\Omega+\alpha_2\int_{{}_t\Omega_2}{}^t\boldsymbol{\tau}({}_t\boldsymbol{u}_2):{}_t\boldsymbol{\eta}(\delta{}_t\boldsymbol{u}_2)\mathrm{d}^t\Omega\\&+\alpha_2\int_{{}_t\Omega_2}{}^t\boldsymbol{\tau}({}_t\boldsymbol{u}_2):{}_t\boldsymbol{e}(\delta{}_t\boldsymbol{u}_2)\mathrm{d}^t\Omega-k\int_{{}^0\Omega_0}({}_t\boldsymbol{u}_1-{}_t\boldsymbol{u}_2)\cdot\delta{}_t\boldsymbol{u}_2\mathrm{d}^0\Omega\\&=\int_{{}_t\Omega_2}\beta_2{}_t^{t+\Delta t}\boldsymbol{f}\cdot\delta{}_t\boldsymbol{u}_2\mathrm{d}^t\Omega,\quad\forall\delta{}_t\boldsymbol{u}_2\in W_2.\end{aligned} \tag{12}$$

In the following, we will use matrix notation to derive the discrete formulation. The Kirchhoff incremental stress ${}_t\boldsymbol{S}_i$ in the domain Ω_i can be rewritten as, with the assumption of isotropic and linear material properties:

$${}_t\boldsymbol{S}_i=\boldsymbol{D}_t\boldsymbol{e}_i, \tag{13}$$

where $\boldsymbol{D}$ is the elasticity matrix.

Now the incremental displacement ${}_t\boldsymbol{u}_i$ in the domain Ω_i is interpolated to give

$${}_t\boldsymbol{u}_i=\boldsymbol{N}_i{}_t\hat{\boldsymbol{u}}_i, \tag{14}$$

where ${}_t\hat{\boldsymbol{u}}_i$ and $\boldsymbol{N}_i$ are, respectively, the nodal incremental displacement and the shape function matrix in the domain Ω_i. Thus the linear and nonlinear incremental strains can be written as follows:

$$ {}_t\boldsymbol{e}_i = {}_t^t\boldsymbol{B}_{\mathrm{iL}}\ {}_t\hat{\boldsymbol{u}}_i, \tag{15} $$

$$ {}_t\boldsymbol{\eta}_i = \frac{1}{2}\,{}_t^t\boldsymbol{A}_i\,{}_t^t\boldsymbol{G}_i\,{}_t\hat{\boldsymbol{u}}_i, \tag{16} $$

where ${}_t^t\boldsymbol{B}_{\mathrm{iL}}$ is the linear strain matrix with respect to domain Ω_i. We then arrive at the relation:

$$ \delta\,{}_t\boldsymbol{\eta}_i = {}_t^t\boldsymbol{A}_i\,{}_t^t\boldsymbol{G}_i\delta\,{}_t\hat{\boldsymbol{u}}_i, \tag{17} $$

where the concrete expressions for ${}_t^t\boldsymbol{A}_i$ and ${}_t^t\boldsymbol{G}_i$ will be given later for the four-node iso-parameter nonlinear element as the consequence of derivation of the tangent stiffness matrix, and the derivation from Eq. (16) to Eq. (17) will be easily found.

Making use of Eqs. (13)–(17), we obtain the discrete forms of Eqs. (11) and (12) in the matrix form:

$$ \left(\begin{bmatrix}\alpha_1\,{}_t^t\boldsymbol{K}_1 & \boldsymbol{0}\\ \boldsymbol{0} & \alpha_2\,{}_t^t\boldsymbol{K}_2\end{bmatrix}+k\begin{bmatrix}\boldsymbol{C}_{11} & -\boldsymbol{C}_{12}\\ -\boldsymbol{C}_{21} & \boldsymbol{C}_{22}\end{bmatrix}\right)\begin{bmatrix}{}_t\hat{\boldsymbol{u}}_1\\ {}_t\hat{\boldsymbol{u}}_2\end{bmatrix} = \begin{bmatrix}\beta_1\,{}_t^{t+\Delta t}\boldsymbol{R}_1\\ \beta_2\,{}_t^{t+\Delta t}\boldsymbol{R}_2\end{bmatrix}-\begin{bmatrix}\alpha_1\,{}_t^t\boldsymbol{F}_1\\ \alpha_2\,{}_t^t\boldsymbol{F}_2\end{bmatrix}, \tag{18} $$

where the tangent stiffness matrix ${}_t^t\boldsymbol{K}_i$ in the domain Ω_i is written as

$$ {}_t^t\boldsymbol{K}_i = {}_t^t\boldsymbol{K}_{\mathrm{iL}} + {}_t^t\boldsymbol{K}_{\mathrm{iNL}}, \tag{19} $$

with the linear and nonlinear components expressed as

$$ {}_t^t\boldsymbol{K}_{\mathrm{iL}} = \int_{{}_t\Omega_i} {}_t^t\boldsymbol{B}_{\mathrm{iL}}^{\mathrm{T}}\boldsymbol{D}\,{}_t^t\boldsymbol{B}_{\mathrm{iL}}\,\mathrm{d}^t\Omega, \tag{20} $$

$$ {}_t^t\boldsymbol{K}_{\mathrm{iNL}} = \int_{{}_t\Omega_i} {}_t^t\boldsymbol{G}_i^T\,{}^t\boldsymbol{\tau}_i\,{}_t^t\boldsymbol{G}_i\,\mathrm{d}^t\Omega, \tag{21} $$

where ${}^t\boldsymbol{\tau}_i$ is the Cauchy stress matrix in the domain Ω_i.

In Eq. (18), ${}_t^t\boldsymbol{F}_i$ is the nodal force of the external work done by the Cauchy stress at time t on the incremental strain:

$$ {}_t^t\boldsymbol{F}_i = \int_{{}_t\Omega_i} {}_t^t\boldsymbol{B}_{\mathrm{iL}}^{\mathrm{T}}\,{}^t\hat{\boldsymbol{\tau}}_i\,\mathrm{d}^t\Omega, \tag{22} $$

where ${}^t\hat{\boldsymbol{\tau}}_i$ is the Cauchy stress vector in domain Ω_i. ${}_t^{t+\Delta t}\boldsymbol{R}_i$ is the equivalent nodal force form of external work:

$$ {}_t^{t+\Delta t}\boldsymbol{R}_i = \int_{{}_t\Omega_i} \boldsymbol{N}_i^{\mathrm{T}}\,\boldsymbol{f}\,\mathrm{d}^t\Omega. \tag{23} $$

$\boldsymbol{C}_{ij}$ is the coupling sub-matrix associated with the incremental displacement:

$$ \boldsymbol{C}_{ij} = \int_{{}_0\Omega_0} \boldsymbol{N}_i^{\mathrm{T}}\boldsymbol{N}_j\ \mathrm{d}^0\Omega. \tag{24} $$

In the following, we will present the tangent stiffness of the four-node iso-parametric element, which is employed in this study. Thus, the displacement field of the coarse or fine element in domain Ω_i can be expressed as

$$ {}_t\boldsymbol{u}_i = \boldsymbol{N}_i\,{}_t\hat{\boldsymbol{u}}_i = \begin{bmatrix}N_1 & 0 & N_2 & 0 & N_3 & 0 & N_4 & 0\\ 0 & N_1 & 0 & N_2 & 0 & N_3 & 0 & N_4\end{bmatrix}{}_t\hat{\boldsymbol{u}}_i, \tag{25} $$

where N_1, N_2, N_3, and N_4 are the standard shape functions, and the nodal incremental displacement ${}_t\hat{\boldsymbol{u}}_i$ can be expressed as

$$ {}_t\hat{\boldsymbol{u}}_i^{\mathrm{T}} = \begin{bmatrix}{}_tu_{i1}^1 & {}_tu_{i2}^1 & \cdots & {}_tu_{i1}^4 & {}_tu_{i2}^4\end{bmatrix}, \tag{26} $$

where ${}_tu_{in}^m$ is the incremental displacement of the mth node in the n direction corresponding to the configuration at time t.

The linear incremental strain can be written as

$$ {}_t\boldsymbol{e}_i = {}_t^t\boldsymbol{B}_{\mathrm{iL}}\,{}_t\hat{\boldsymbol{u}}_i, \tag{27} $$

where the linear incremental strain matrix ${}_t^t\boldsymbol{B}_{\mathrm{iL}}$ is given by

$$ {}_t^t\boldsymbol{B}_{\mathrm{iL}} = \begin{bmatrix}{}_tN_{i1,x} & 0 & \cdots & {}_tN_{i4,x} & 0\\ 0 & {}_tN_{i1,y} & \cdots & 0 & {}_tN_{i4,y}\\ {}_tN_{i1,y} & {}_tN_{i1,x} & \cdots & {}_tN_{i4,y} & {}_tN_{i4,x}\end{bmatrix}, \tag{28} $$

where ${}_tN_{im,x(y)}$ is the derivative of the standard shape function ${}_tN_{im}$ (m=1–4) in the domain Ω_i with respect to the coordinate x(y) corresponding to the configuration at time t.

The nonlinear incremental strain ${}_t\boldsymbol{\eta}_i$ can be written as

$$
\begin{aligned}
{}_t\boldsymbol{\eta}_i &= \frac{1}{2}\,{}_t^t\boldsymbol{A}_i\left[\,{}_tu_{i1,x}\quad {}_tu_{i1,y}\quad {}_tu_{i2,x}\quad {}_tu_{i2,y}\,\right]^{\mathrm{T}}\\
&=\frac{1}{2}\begin{bmatrix} {}_tu_{i1,x} & 0 & {}_tu_{i2,x} & 0\\ 0 & {}_tu_{i1,y} & 0 & {}_tu_{i2,y}\\ {}_tu_{i1,y} & {}_tu_{i1,x} & {}_tu_{i2,y} & {}_tu_{i2,x}\end{bmatrix}\begin{bmatrix} {}_tu_{i1,x}\\ {}_tu_{i1,y}\\ {}_tu_{i2,x}\\ {}_tu_{i2,y}\end{bmatrix},
\end{aligned}
\tag{29}
$$

and we have

$$
\begin{aligned}
\left[\,{}_tu_{i1,x}\quad {}_tu_{i1,y}\quad {}_tu_{i2,x}\quad {}_tu_{i2,y}\,\right]^{\mathrm{T}} &= {}_t^t\boldsymbol{G}_i\,{}_t\hat{\boldsymbol{u}}_i\\
&=\begin{bmatrix} {}_tN_{i1,x} & 0 & \cdots & {}_tN_{i4,x} & 0\\ {}_tN_{i1,y} & 0 & \cdots & {}_tN_{i4,y} & 0\\ 0 & {}_tN_{i1,x} & \cdots & 0 & {}_tN_{i4,x}\\ 0 & {}_tN_{i1,y} & \cdots & 0 & {}_tN_{i4,y}\end{bmatrix}{}_t\hat{\boldsymbol{u}}_i,
\end{aligned}
\tag{30}
$$

where ${}_tu_{in,x(y)}$ is the derivative of the component ${}_tu_{in}$, (n=1, 2) of the incremental displacement in the domain Ω_i with respect to the coordinate x(y) corresponding to the configuration at time t. From the concrete expressions for ${}_t^t\boldsymbol{A}_i$ in Eq. (29) and ${}_t^t\boldsymbol{G}_i$ in Eq. (30) as well as the Cauchy stress matrix ${}^t\boldsymbol{\tau}_i$ at time t, the tangent stiffness can be derived directly using Eqs. (19)–(21).

With the above formulations, the coupling sub-matrix $\boldsymbol{C}_{ij}$ can be computed via Gaussian quadrature rules according to the proposed unified method for calculating the coupling matrices (Qiao *et al.*, 2011).

3 Arlequin user element

In this section, we consider the coupling of two four-node iso-parametric elements to show the implementation of the penalty-based Arlequin method into ABAQUS.

We define the four-node iso-parametric element with nodes C_1 to C_4 as the coarse element, and that with nodes F_1 to F_4 as the fine element (Fig. 3). Here the penalty method is used to couple the coarse and fine elements. The coupling of the fine and coarse elements can be realized through the combination of two user defined elements in ABAQUS. One user element is contributed to the geometric nonlinear effect, and the other is only responsible for the Arlequin coupling effect, and both will be discussed in the following.

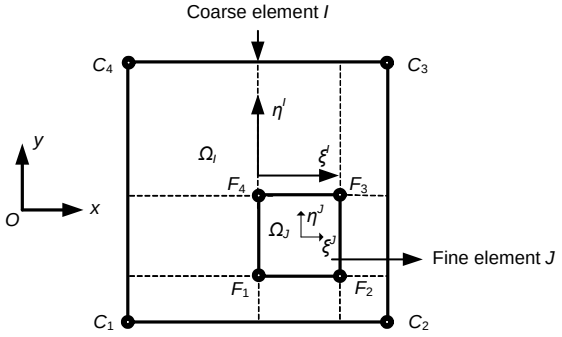

Fig. 3 Coupling of coarse element *I* and fine element *J* using the penalty method

$\eta^{I(J)}$ and $\xi^{J(I)}$ are reference coordinates of the coarse and fine elements

Both user elements 1 and 2 are virtual elements, consisting of the same set of eight nodes (i.e., F_1, F_2, F_3, F_4, C_1, C_2, C_3, and C_4). According to the ABAQUS manual, we should define the tangent stiffness matrix AMATRX for the nonlinear analysis. In our analysis, we define the two user elements as

$$
\mathrm{AMATRX}_{\mathrm{UEL}_1}=\begin{bmatrix}\alpha_I\,{}_t^t\boldsymbol{K}_I & 0\\ 0 & \alpha_J\,{}_t^t\boldsymbol{K}_J\end{bmatrix},
\tag{31}
$$

$$
\mathrm{AMATRX}_{\mathrm{UEL}_2}=k\begin{bmatrix}\boldsymbol{C}_{II} & -\boldsymbol{C}_{IJ}\\ -\boldsymbol{C}_{JI} & \boldsymbol{C}_{JJ}\end{bmatrix},
\tag{32}
$$

where $\boldsymbol{C}_{IJ}$ in Eq. (32) is associated with the penalty-based Arlequin coupling, which can be found in Eq. (18) with the subscript 1(2) replaced by $I(J)$. ${}_t^t\boldsymbol{K}_J$ and ${}_t^t\boldsymbol{K}_I$ are the un-weighted tangent stiffness matrices of the fine and coarse elements at time t, and α_J and α_I ($\alpha_J+\alpha_I=1$) are the weight functions of the fine and coarse elements, respectively.

As explained in the ABAQUS manual, the right-hand side should be treated carefully in the nonlinear analysis. According to Eq. (18), the right-hand side of the user element UEL_1 is written as

$$\mathrm{RHS}_{\mathrm{UEL}_1} = \mathrm{RHS}_{\mathrm{UEL}_1} - \begin{bmatrix} \alpha_I \, {}_t^t\boldsymbol{F}_I \\ \alpha_J \, {}_t^t\boldsymbol{F}_J \end{bmatrix}, \quad (33)$$

where ${}_t^t\boldsymbol{F}_{I(J)}$ is the equivalent nodal force vector of the work done by the Cauchy stress over the incremental strain, which can be found from Eq. (22) with the subscript i replaced by $I(J)$. The right-hand side of the user element UEL_2 is not related to the geometric nonlinear residual, and can be expressed as

$$\mathrm{RHS}_{\mathrm{UEL}_2} = \mathrm{RHS}_{\mathrm{UEL}_2} - \mathrm{AMATRX}_{\mathrm{UEL}_2} \times \boldsymbol{U}_{\mathrm{UEL}_2}, \quad (34)$$

where $\boldsymbol{U}_{\mathrm{UEL}_2}$ is the nodal incremental displacement vector of the user defined element UEL_2.

The coupling matrices corresponding to the configuration at time 0 are always constant during the nonlinear solution procedure. Thus, the geometrical nonlinear effect and the Arlequin coupling effect should be separated from each other. This separation is also helpful for the nonlinear convergence check in ABAQUS standard.

4 Numerical verification

In this section, we will present two numerical examples to verify the accuracy of the proposed Arlequin framework. CPS4 elements provided by ABAQUS are used in the two examples, and the user element is employed to couple the fine and coarse elements in the coupling zone. The constant weight functions of the fine and coarse elements in the coupling zone are adopted and taken to be 0.9 and 0.1, respectively. A narrow coupling length should be used to minimize the effect of the Arlequin model on the regions outside of the coupling zone (Guidault and Belytschko, 2007). The external force will be loaded using 100 increments, and the load factor of each increment is 0.01. The maximum number of iterations for each increment is set to be 3. The modified Newton-Raphson method is employed in ABAQUS standard.

We set the penalty parameter to be $k=\alpha\times K_{\max}$, where α is an integer, and $K_{\max}$ is the maximum stiffness coefficient in the linear stiffness matrix of the coarse element in the coupling zone. The results calculated from the coupled model with $k\geq 100K_{\max}$ are almost the same for the large constraints. Thus, only those from the coupled model with $k=100K_{\max}$ are listed in the two examples. It is noted here that the penalty parameter in the conventional penalty-based finite element analysis is usually chosen to be a very large number, i.e., $k=10^6K_{\max}$, which is determined also based on trial experiments (Chandrupatla and Belegundu, 1991). However, the penalty parameter in the Arlequin framework shall not be too large in order to avoid negating the energy partition effect as indicated in Eqs. (1)–(4).

We first considered a cantilever beam with the left end clamped, which is subjected to uniform pressure p=5 N/cm on the top of the beam, as shown in Fig. 4. The geometric parameters are taken as L=10 cm, h=1 cm, and b=1 cm while the Young's modulus and the Poisson's ratio are E=12 000 N/cm^2 and ν=0.2, respectively. The plane-stress state with a unit thickness is assumed.

For the sake of comparison, we established two mono-models (fine and coarse models) and a coupled model. The coupled model is shown in Fig. 5. The length of the coupling zone is taken to be 0.25 cm.

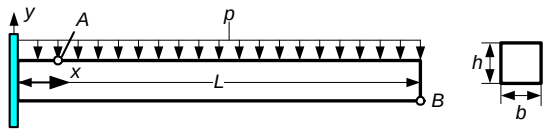

Fig. 4 A cantilever beam subjected to uniform pressures
p is the external uniform pressure; L, h, and b are the length, height, and width of the beam, respectively

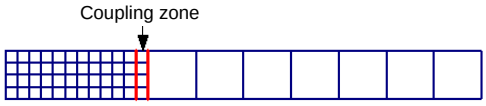

Fig. 5 Sketch for the coupled model

Figs. 6 and 7 display, respectively, the relationship between the transverse displacement at point B (10, −0.5) and the normal stress at point A (1, 0.5) and the dimensionless load. For comparison, we show the solutions obtained using the coarse, fine, and coupled models using various penalty parameters, i.e., $k=\alpha\times K_{\max}$ ($K_{\max}\approx 1.7\times 10^4$). From Figs. 6 and 7, we can conclude that the coupled model with $k=K_{\max}$ is not able to yield reliable results due to the insufficient constraints, and the results of the coupled model with $k=10K_{\max}$ or $k=100K_{\max}$ seem to be more reasonable as compared with the fine model.

Second, we studied the static buckling of a shallow arch with two hinged ends subjected to prescribed displacement at point *B*, as shown in Fig. 8. The geometric parameters are taken as *D*=36 cm, *h*=1.5 cm, *H*=1.0 cm, and *R*=162.5 cm. The Young's modulus and the Poisson's ratio are *E*=100 000 N/cm^2 and *v*=0.3, respectively. The plane-stress state with a unit thickness is also assumed.

We established two mono-models (fine and coarse models) and a coupled model. The coupled model is shown in Fig. 9, for which the penalty-based Arlequin method is employed to couple the fine and coarse elements in the coupling zone.

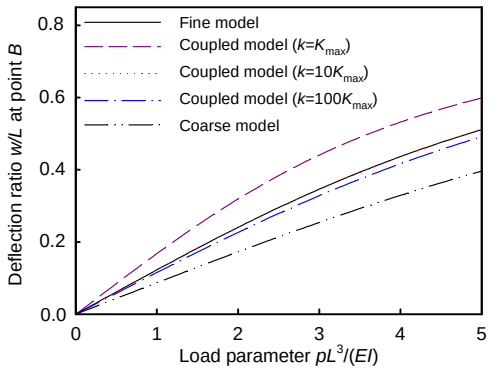

Fig. 6 Deflection at point *B* vs. the dimensionless load
I is the inertial moment of the cross-section

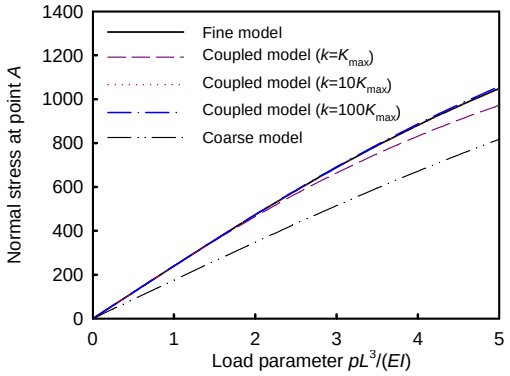

Fig. 7 Normal stress at point *A* vs. the dimensionless load

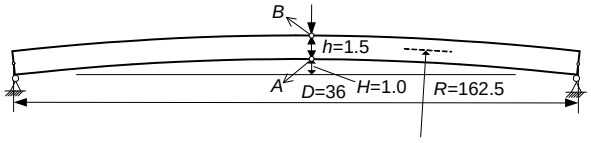

Fig. 8 A shallow arch subjected to prescribed displacement
D: distance between two hinged points, cm; *R*: radius of the circular arch, cm; *h*: height of the cross-section, cm; *H*: distance from the hinge level to the bottom of middle-span section, cm

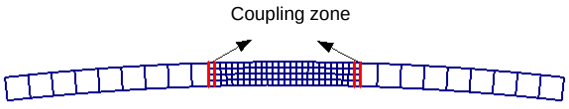

Fig. 9 Sketch for the coupled model

Figs. 10 and 11 show, respectively, the vertical reaction force at point *B* and the normal stress at point *A* vs. the transverse deflection at the load point. From Fig. 10, one can observe that the results calculated from the coupled model with $k=K_{max}$ ($K_{max}\approx1.5\times10^5$) become inaccurate for large displacement. The corresponding results from the coupled model with other penalty parameters always fall in between those calculated from the coarse and fine models. From Fig. 11, one can see that the normal stress of the coupled model with $k=K_{max}$ is obviously unreasonable due to insufficient constraints, and the results of the coupled model with $k=10K_{max}$ are more accurate than those of the coupled models with $k=20K_{max}$ and $k=100K_{max}$ when compared with the fine model.

From the two numerical examples, one can conclude that the penalty version of Arlequin framework can be employed to obtain reasonably accurate stresses when the penalty parameter is chosen properly. From our simulation, the value of $k\approx10K_{max}$ is recommended.

For the comparison of numerical efficiency, the total number of variables in the fine and coupled models for the two numerical examples is listed in Table 1, along with numbers of elements and nodes. CPU times consumed are not reported here due to the very short time necessary to solve these two simple problems. Nevertheless, Table 1 clearly illustrates a higher efficiency of the global/local analysis based on the Arlequin framework. Thus, the global/local geometric nonlinear simulation using the Arlequin framework based on the ABAQUS platform will lead to a lower computational cost while maintaining an acceptable accuracy.

Table 1 Numerical aspects between different models

Aspect	Example 1		Example 2	
	Fine model	Coupled model	Fine model	Coupled model
NOE	160	65	384	142
NON	205	83	485	179
TNOV	410	166	970	358

NOE: number of elements; NON: number of nodes; TNOV: total number of variables

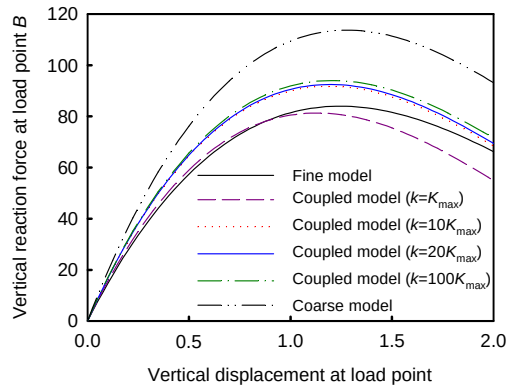

Fig. 10 Vertical reaction force vs. the vertical displacement at point *B*

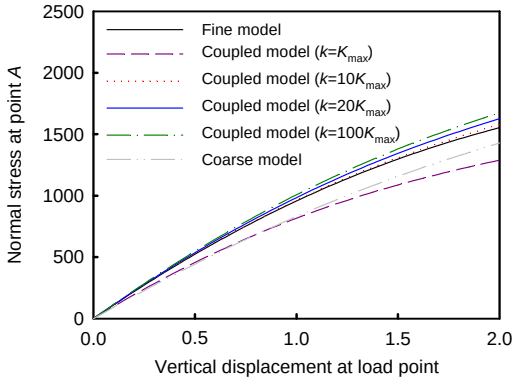

Fig. 11 Normal stress at point *A* vs. the vertical displacement at point *B*

5 Conclusions

In this paper, we considered the geometric nonlinear global/local analysis of structures by virtue of the ABAQUS platform. The penalty-based Arlequin framework was employed and investigated as an efficient global/local analysis strategy. Some issues related to the implementation of the method into ABAQUS were discussed. Numerical results show that the global/local technique based on the penalty version of the Arlequin framework can be employed to capture the exact stresses of interest with a lower cost when an appropriate penalty parameter is adopted.

Two issues, which are particularly critical to the implementation of the Arlequin method into ABAQUS, should be mentioned. First, the coupling matrix should be formulated according to the configuration at time 0 in the nonlinear analysis. In addition, the coupling effect can be separated from the geometrical nonlinear effect during the definition of the ABAQUS user elements. Bearing these in mind, one can use this global/local analysis method to solve more complex problems involving large deformation based on the ABAQUS platform.

References

Bathe, K.J., 1996. Finite Element Procedures. Prentice Hall, USA.

Ben Dhia, H., 1998. Multiscale mechanical problems: the Arlequin method. *Comptes Rendus de l'Académie des Sciences-Series IIB-Mechanics-Physics-Astronomy*, **326**(12):899-904 (in French). [doi:10.1016/S1251-8069(99)80046-5]

Ben Dhia, H., 2008. Further insights by theoretical investigations of the multi-scale Arlequin method. *International Journal for Multiscale Computational Engineering*, **6**(3):215-232. [doi:10.1615/IntJMultCompEng.v6.i3.30]

Ben Dhia, H., Rateau, G., 2001. Analyse mathématique de la méthode arlequin mixte. *Comptes Rendus de l'Académie des Sciences-Series I-Mathematics*, **332**(7):649-654 (in French). [doi:10.1016/S0764-4442(01)01900-0]

Ben Dhia, H., Zammali, C., 2004. Level-sets and Arlequin framework for dynamic contact problems. *Finite Elements European Review*, **5-7**(13):403-414.

Ben Dhia, H., Rateau, G., 2005. The Arlequin method as a flexible engineering design tool. *International Journal for Numerical Methods in Engineering*, **62**(11):1442-1462. [doi:10.1002/nme.1229]

Chandrupatla, T.R., Belegundu, A.D., 1991. Introduction to Finite Elements in Engineering. Prentice-Hall, USA.

Fish, J., 1992. The s-version of the finite element method. *Computers and Structures*, **43**(3):539-547. [doi:10.1016/0045-7949(92)90287-A]

Guidault, P.A., Belytschko, T., 2007. On the L^2 and the H^1 couplings for an overlapping domain decomposition method using Lagrange multipliers. *International Journal for Numerical Methods in Engineering*, **70**(3):322-350. [doi:10.1002/nme.1882]

Hu, H., Belouettar, S., Potier-Ferry, M., Daya, E.M., 2008. Multi-scale modelling of sandwich structures using the Arlequin method Part I: linear modelling. *Finite Elements in Analysis and Design*, **45**(1):37-51. [doi:10.1016/j.finel.2008.07.003]

Hu, H., Belouettar, S., Potier-Ferry, M., Daya, E.M., Makradi, A., 2010. Multi-scale nonlinear modelling of sandwich structures using the Arlequin method. *Composite Structures*, **92**(2):515-522. [doi:10.1016/j.compstruct.2009.08.051]

Hughes, T.J.R., 1995. Multiscale phenomena: Green's functions, the Dirichlet-to-Neumann formulation, subgrid scale models, bubbles and the origins of stabilized methods. *Computer Methods in Applied Mechanics and*

Engineering, **127**(1-4):387-401. [doi:10.1016/0045-7825(95)00844-9]

Qiao, H., Chen, W.Q., Zhang, C.Z., 2010. Dynamic Multiscale Analysis of Structures via the ARLEQUIN Method. Proceedings of the 1st International Conference on Advances in Interaction and Multiscale Mechanics, Jeju, Korea.

Qiao, H., Yang, Q.D., Chen, W.Q., Zhang, C.Z., 2011. Implementation of the Arlequin method into ABAQUS: basic formulations and applications. *Advances in Engineering Software*, **42**(4):197-207. [doi:10.1016/j.advengsoft.2011.02.005]

Rannou, J., Gravouil, A., Baietto-Dubourg M. C., 2009. A local multigrid X-FEM strategy for 3-D crack propagation. *International Journal for Numerical Methods in Engineering*, **77**(4):581-600. [doi:10.1002/nme.2427]

Voleti, S.R., Chandra, N., Miller, J.R., 1996. Global-local analysis of large-scale composite structures using finite element methods. *Computers and Structures*, **58**(3):453-464. [doi:10.1016/0045-7949(95)00172-D]

Whitcomb, J.D., Woo, K., 1993. Application of iterative global/local finite element analysis. Part 1: linear analysis. *Communications in Numerical Methods in Engineering*, **9**(9):745-756. [doi:10.1002/cnm.1640090905]